Since January 2020 Elsevier has created a COVID-19 resource centre with free information in English and Mandarin on the novel coronavirus COVID-19. The COVID-19 resource centre is hosted on Elsevier Connect, the company's public news and information website.

Diamond & Related Materials 134 (2023) 109775

Contents lists available at ScienceDirect

Diamond & Related Materials

journal homepage: www.elsevier.com/locate/diamond

Trace detection of SARS-CoV-2 N-protein by diamond solution-gate field-effect transistor

Qianwen Zhang [a], Minghui Zhang [a], Yuxiang Du [a], Bangqiang Xu [b], Genqiang Chen [a], Shi He [a], Dan Zhang [b], Qi Li [a], Hong-Xing Wang [a,*]

[a] The Key Laboratory of Physical Electronics and Devices, Ministry of Education, School of Electronic Science and Engineering, Xi'an Jiaotong University, Xi'an, Shaanxi 710049, China

[b] Laboratory of Infectious and Immune Diseases, Shaanxi Provincial People's Hospital (The Third Affiliated Hospital of Xi'an Jiaotong University), Xi'an 710068, China

ARTICLE INFO

Keywords:
Diamond
Solution-gate field-effect transistor
SARS-CoV-2 N-protein
Biosensor

ABSTRACT

In this study, we introduced H-terminated diamond solution-gate field-effect transistor (H-diamond SGFET) to detect trace SARS-CoV-2 N-protein, which plays an important role in replication and transcription of viral RNA. 1-Pyrenebutyric acid-N-hydroxy succinimide ester (Pyr-NHS) was modified on H-diamond surface as linker, on which the specific antibody of SARS-CoV-2 N-protein was catenated. Fourier transform infrared spectrum, scanning electron microscope and energy dispersive spectrum were utilized to demonstrate the modification of H-diamond with Pyr-NHS and antibody. Shifts of $I_{DS(max)}$ at $V_{GS} = -500$ mV in transfer characteristics of H-diamond SGFET was observed to determine N-protein concentration in phosphate buffer solution. Good linear relationship between $I_{DS(max)}$ and $\log_{10}$(N-protein) was observed from 10^{-14} to 10^{-5} g/mL with goodness of fit $R^2 = 0.90$ and sensitivity of 1.98 μA/Log_{10} [concentration of N-protein] at $V_{DS} = -500$ mV, $V_{GS} = -500$ mV. Consequently, this prepared H-diamond SGFET biosensor may provide a new idea for diagnosis of SARS-CoV-2 due to a wide detection range from 10^{-14} to 10^{-5} g/mL and low limit of detection 10^{-14} g/mL.

1. Introduction

Since 2019, the severe acute respiratory syndrome coronavirus 2 (SARS-CoV-2) has become a major global public health event [1], and it still seriously affects the healthy life and daily affairs of human beings. It is important to explore effective method for detection of SARS-CoV-2, which could reduce virus transmission [2]. Nucleic acid detection is the primary standard for diagnosing viral diseases and plays a significant role in prevention and control of SARS-CoV-2 [3]. However, it has some shortcomings such as long time, high cost, and the waste of manpower and physical resources. It is necessary to develop a timely and effective method for diagnosis of SARS-CoV-2 to control its spread. Antigen assay is another important technology for diagnosis of SARS-CoV-2, and it is an effective and trustworthy diagnosis method [4]. As for SARS-CoV-2, it consists of four structural proteins: spike protein (S), envelope protein (E), membrane glycoprotein (M) and nucleocapsid protein (N) [5]. Among them, Nucleocapsid protein (N-protein) is a highly immunogenic phosphoprotein and a multifunctional RNA-binding protein, which is necessary for viral RNA replication and transcription [6]. It has been reported that N-protein is a promising structural protein for antigen detection of SARA-Cov-2 [7–9]. Therefore, several methods have been developed for antigen assay including N-protein detection. With the development of electronic devices, field-effect transistors have been widely applied in the area of antigen assay [10–12].

As for diamond, wide bandgap (5.5 eV), high carrier mobility (3800 and 4500 $\text{cm}^2\,\text{V}^{-1}\,\text{s}^{-1}$ for electron and hole), high thermal conductivity (2200 $\text{W m}^{-1}\,\text{K}^{-1}$) and high breakdown electric field (>10 MV/cm) [13] make it an excellent material for field-effect transistors. What's more, it has excellent electrochemical properties including wide electrochemical potential window and strong biocompatibility [14]. As a result, diamond electronic devices have been extensively developed to apply in biosensing [14,15]. For Si-based ion sensitive field effect transistor, a thick dielectric layer is needed to passivate the surface from being oxidized, resulting a decrease in sensing response and sensitivity [16]. However, diamond SGFET surface is directly connected with electrolyte without insulated layer, a higher sensitivity was obtained. In addition, it is a great challenge for graphene-FET and carbon nanotubes-FET to avoid surface contamination in practical application due to their larger

* Corresponding author.
E-mail address: hxwangcn@mail.xjtu.edu.cn (H.-X. Wang).

https://doi.org/10.1016/j.diamond.2023.109775
Received 7 November 2022; Received in revised form 8 February 2023; Accepted 8 February 2023
Available online 11 February 2023

specific area [17]. Therefore, diamond SGFET is an excellent alternative for biosensor.

In this study, H-terminated diamond solution-gate field-effect transistor (H-diamond SGFET) was introduced to detect trace SARS-CoV-2 N-protein.

2. Experimental

Fig. 1 showed the schematic diagram of H-diamond SGFET for detecting SARS-CoV-2 N-protein. Firstly, high temperature high pressure diamond substrate was cleaned by a mixture of sulfuric acid and nitric acid with ratio of 1:3. Then, 500 nm diamond epitaxial layer was grown by microwave plasma chemical vapor deposition and treated by hydrogen-rich microwave plasma, resulting a H-terminated diamond surface. The detailed information can be found in our previous work [18]. Next, 200 nm Au film was deposited on H-diamond as source and drain electrodes to form ohmic contact by electron beam evaporation system. After that, ultraviolet radiation was utilized to isolate electronic connections for FET with channel area covered by photoresist. Then, source and drain electrodes were packaged by epoxy resin to protecting them from electrolyte solution. Next is the modification of H-diamond surface. Linker 1-pyrenebutyric acid-N-hydroxy succinimide ester (Pyr-NHS) was dissolved in methanol and dropped in the sensing area in conductive channel, followed by standing for 2 h at room temperature. After that, the specific antibody of N-protein dissolved in phosphate buffer solution (PBS) was dropped in the sensing area and incubated at 4 °C for 2 h, then dried by nitrogen flow.

The morphology of modified diamond was characterized by scanning electron microscopy (SEM) using a model Quanta 250 FEG (FEI Company), and the molecular groups modified on diamond surface were measured by fourier transform infrared spectrometer (FT-IR) using a diffuse reflection model (Thermo Nicolet IS 50). The electrical characteristics of the prepared diamond SGFET were measured by a power device analyzer (Agilent Technologies B1505A).

In order to investigate the performance of H-diamond SGFET for detecting trace SARS-CoV-2 N-protein, SARS-CoV-2 N-protein was diluted into different concentrations from 10^{-14} to 10^{-5} g/mL by PBS solution, and then dripped into the sensing area. I-V characteristics were measured in a beaker with PBS solution by immersing biosensor and reference electrode in solution. After the detection of each concentration of N-protein, glycine was utilized to dissociate the binding of SARS-CoV-2 N-protein and specific antibody, then the biosensor was rinsed with PBS solution and dried by nitrogen gas flow. Next, another concentration of N-protein was dropped on sensing area in this biosensor for concentration detecting.

3. Results and discussion

Fourier transform infrared spectrum (FT-IR) of functionalized H-diamond was exhibited in Fig. 2, which provided evidence for the presence of Pyr-NHS and antibody on H-diamond surface. The broad IR peak in 3200–3500 cm^{-1} was observed assigned to the stretching modes of H_2O [19]. The sharp peak at 847 cm^{-1} was attributed to the vibration of C—H in pyrene ring in Pyr-NHS [20], and the two peaks near 2035 and 2157 cm^{-1} was due to benzene ring and its derivative in Pyr-NHS. The peak in 1630 and 1305 cm^{-1} could be observed due to amide I bond and amide III bond in N-protein antibody [21], and exhibited α-helical characteristic structure [22]. Moreover, the linker Pyr-NHS and antibodies were bound by this amide bond. Two weak peaks near 2500 cm^{-1} were due to the hydroxyl stretches arising from the carboxyl group in specific antibody [19]. Therefore, these results indicated that the H-diamond surface was modified with Pyr-NHS and antibody.

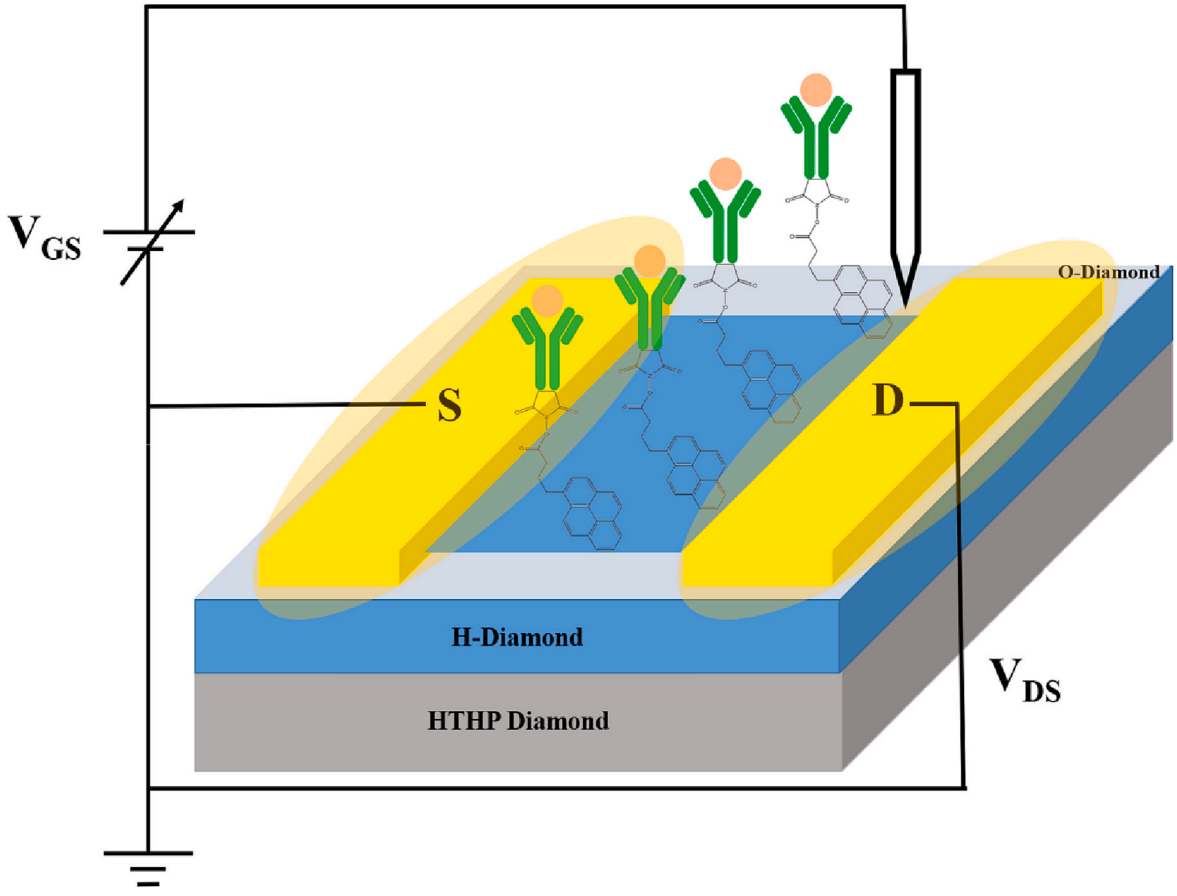

Fig. 1. Schematic diagram of H-diamond SGFET for detecting SARS-CoV-2 N-protein.

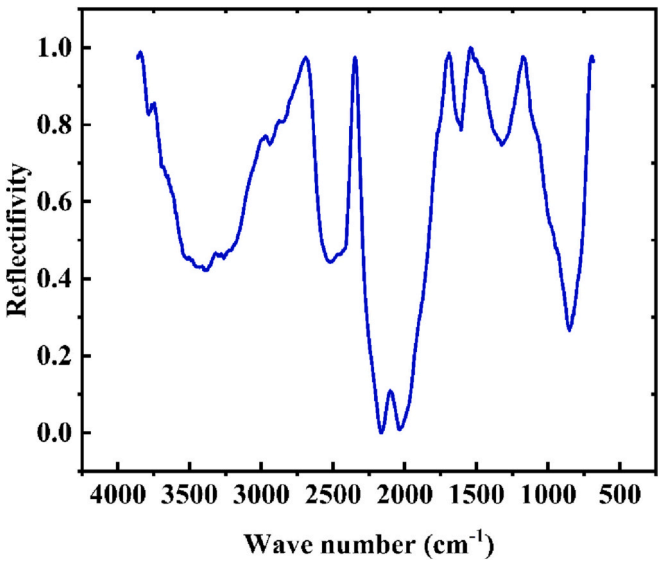

Fig. 2. FT-IR spectrum of modified H-diamond SGFET.

Fig. 3 showed the SEM images of modification process of H-diamond. Fig. 3(a) exhibited a flat surface of H-diamond. After modified by Pyr-NHS, a few thin film textures were observed in Fig. 3(b). After the modification of antibody, some massive tissues appeared on diamond surface due to the combination of antibody and Pyr-NHS. In addition, the measurement environment of SEM was room temperature, which was higher than the storage temperature of protein, some antibodies may aggregate on H-diamond surface to form floccules and lumps [23], as shown in Fig. 3(c).

SEM image of the scanning field of view of EDS spectrum was shown in Fig. 4(a). And EDS spectrum of N element mapping, O element mapping, C element mapping were exhibited in Fig. 4(b)–(d). The four vertices of the square in Fig. 4 corresponded to the aggregates in SEM image, and its corresponding positions in N mapping, O mapping, and C mapping in the EDS spectrum. In the corresponding area in Fig. 4(b)–(d), C elements were seriously missing, O elements were most densely distributed, and N elements were sparsely distributed. This could be attributed to the appearance of specific antibody on diamond surface. Compared with H-diamond, the content of N element and O element increased greatly in modified diamond. And this was demonstrated in EDX spectrum for H-diamond, Pyr-NHS/diamond, antibody/Pyr-NHS/diamond and the comparation of XPS spectrum in supplementary material. Therefore, SEM image, EDS mapping and XPS spectrum could confirm the modification of H-diamond surface.

The electronic characterization of H-diamond SGFET was exhibited in Fig. 5. The output curves of H-diamond SGFET was shown in Fig. 5(a), with gate-source voltage (V_{GS}) varying from 200 to −800 mV in steps of −200 mV. The width (W_G) and length (L_G) of conductive channel were 2020 μm and 220 μm, respectively. Drain-source current (I_{DS}) negatively increased as V_{GS} negatively increased, which was consistent with p-type conductive channels of H-diamond. The maximum I_{DS} ($I_{DS(max)}$) was −267.6 μA, obtained as V_{GS} = −800 mV, V_{DS} = −800 mV. The transfer characteristics of H-diamond SGFET after each modification process were investigated in Fig. 5(b). A significant reduction in current I_{DS} was observed due to the decrease of hole carrier density. This could be attributed to the reduction of the conductive channel area of H-diamond because of the attachment of Pyr-NHS layer on surface. The absorption on H-diamond surface could significantly influence the electron emission properties [24], resulting an effect on transconductance and current of device. However, I_{DS} in transfer characteristics increased after the specific antibody linked on Pyr-NHS. This indicated that the antibody was negatively charged, which decreased the holes carrier density and led to the reduction of transconductance. Therefore, the value of I_{DS} changed after each modification process due to the change of holes carrier density. These results confirmed the modification of H-diamond SGFET surface.

Fig. 6(a) exhibited the transfer characteristics of device with various concentrations (10^{-14}–10^{-5} mg/mL) of N-protein at V_{DS} = −500 mV, V_{GS} = 400 to −500 mV. The gate current density at open state was 10^{-5}–10^{-4} mA/mm, which is almost the same order of magnitude as other H-diamond FETs [25,26]. A consecutive decrease of maximum source-drain current ($I_{DS(max)}$) was observed from −44.69 to −23.69 μA, with N-protein concentration increasing from 10^{-14}–10^{-5} g/mL. This decrease in current was attributed to the reduction of hole carrier density in p-type conductive channels, which made the transconductance of H-diamond SGFET decrease. According to the literature [27], SARS-CoV-2 N-protein is composed of 419 amino acids with a molecular formula of $C_{1971}H_{3137}N_{607}O_{627}S_7$, and the isoelectric point is 10.07, resulting that N-protein is positively charged in PBS solution (pH = 7.4). The specific binding between N-protein and antibody provided extra positive charge in the interface of diamond and electrolyte, which influenced the carrier density in channels. When the concentration of N-protein increased, the holes carrier density in p-type conductive channels reduced, and then the transconductance of H-diamond decreased. Therefore, the $I_{DS(max)}$ decreased with the increase of N-protein concentration. The values of $I_{DS(max)}$ were investigated in Fig. 6(b) and linearly fitted corresponding to Log_{10} [concentration of N-protein]. The values of $I_{DS(max)}$ was dependent on N-protein concentration and linearly reduced as N-protein increasing with a goodness of fit R^2 = 0.90. The sensitivity of N-protein detection could be obtained as 1.98 μA/Log_{10} [concentration of N-protein] by the slope of linear fitting curve. Consequently, the concentration of N-protein could be obtained from

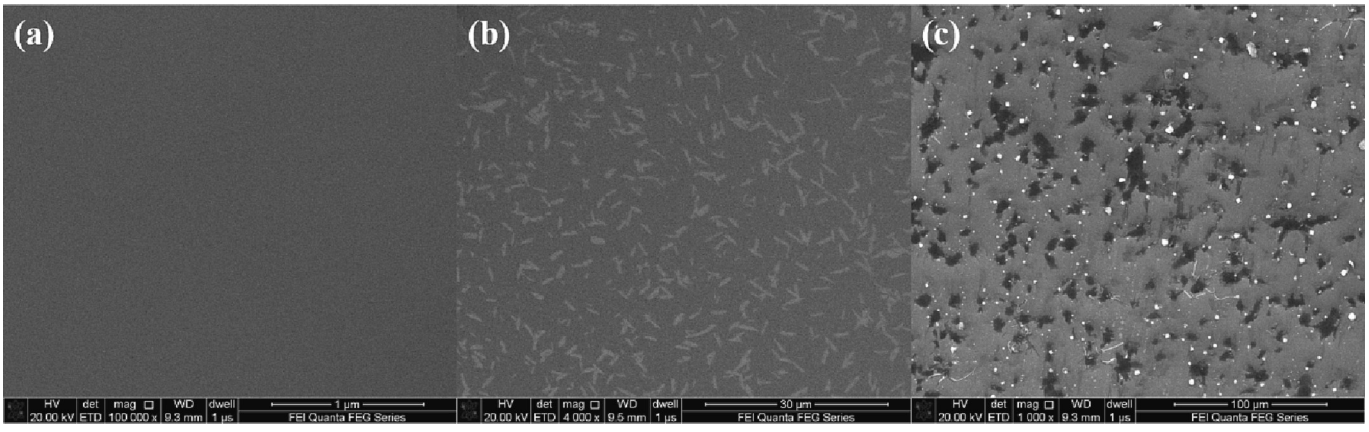

Fig. 3. SEM images of modification process: (a) H-diamond; (b) H-diamond modified with Pyr-NHS; (c) H-diamond modified with Pyr-NHS and antibody.

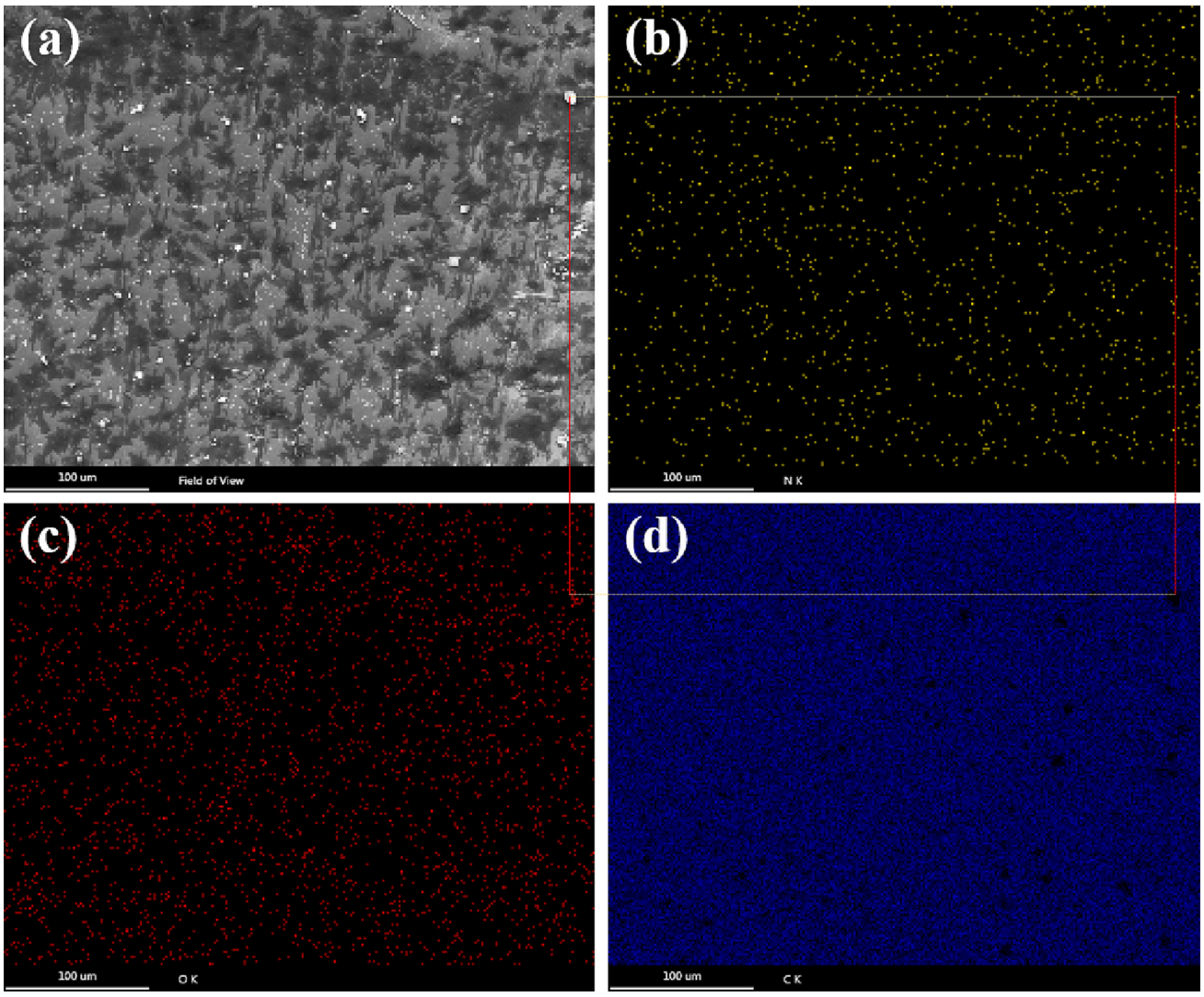

Fig. 4. (a) The scanning field of view of EDS; EDS spectrum of (b) N element mapping (c) O element mapping and (d) C element mapping on modified H-diamond surface.

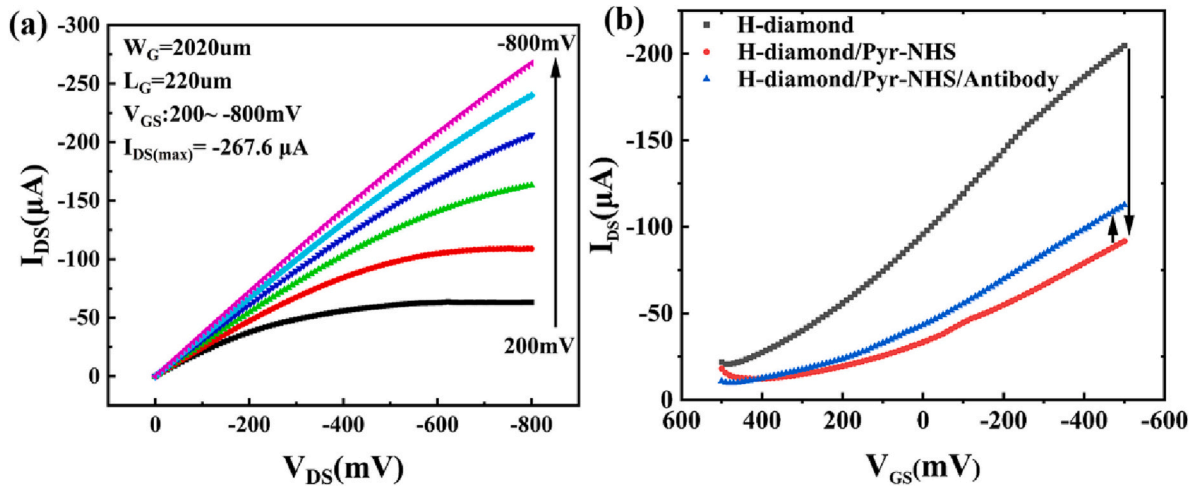

Fig. 5. Performance of H-diamond SGFET: (a) output characteristics of device; (b) transfer characteristics of device in each modification process.

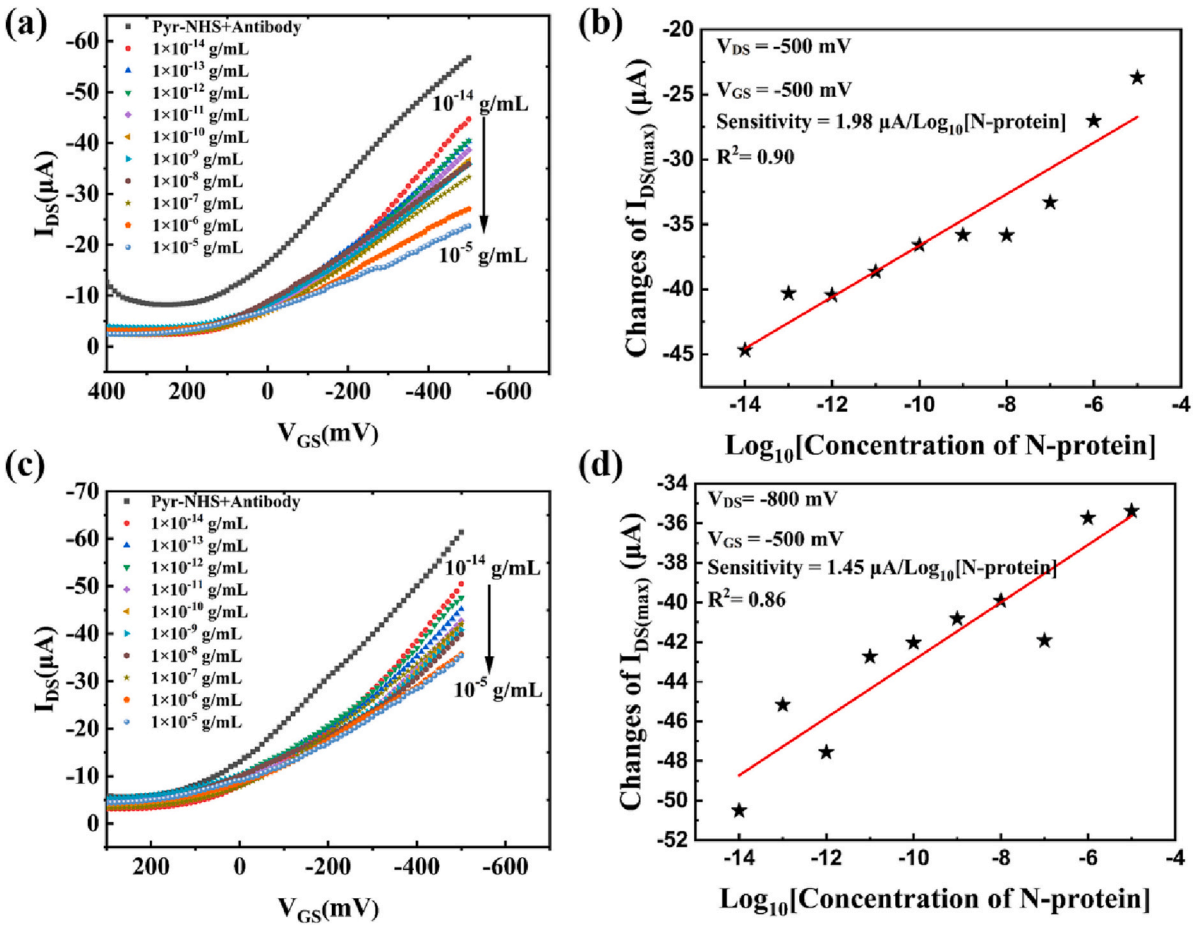

Fig. 6. Detection of SARS-CoV N-protein by H-diamond SGFET: (a) transfer characteristics of device with different concentrations of N-protein at V_{DS} = −500 mV, V_{GS} = 400 to −500 mV and (b) linear fitting curve for $I_{DS(max)}$ and lg(N-protein antigen) for the corresponding conditions; (c) transfer characteristics of device at V_{DS} = −800 mV, V_{GS} = 300 to −500 mV and (d) linear fitting curve for $I_{DS(max)}$ and lg(N-protein antigen) for the corresponding conditions.

the linear relationship between values of $I_{DS(max)}$ and Log10 [concentration of N-protein]. Noting that the sensitivity of biosensor could be improved by optimizing surface density of antibody, as reported in previous papers [28,29]. Also, an appropriate surface antibody density is required to ensure the conductivity and sensitivity of H-diamond biosensor due to the surface absorption of H-diamond [30]. Similarly, Fig. 6(c) depicted the transfer characteristics of device with different concentrations of N-protein at another voltage condition: V_{DS} = −800 mV, V_{GS} = 300 to −500 mV. When the concentration of N-protein increasing from 10^{-14} to 10^{-5} g/mL, values of $I_{DS(max)}$ decreased from −50.51 to −35.39 μA in transfer characteristics. The values of $I_{DS(max)}$ and Log_{10}[N-protein concentration] exhibited linear relationship with goodness of fit R^2 = 0.86, sensitivity of 1.45 μA/Log_{10} [concentration of N-protein]. This was also due to the reduction of holes in conductive channels, which effected by the charge density at solid-liquid interface.

The reduced hole carrier density (ΔQi) can be determined by formula (1). ΔQh is the extra charge appears at solid-liquid interface, Ci is the channel surface capacitance of solid side and Cdl is the electric double-layer capacitance of electrolyte [16]. Here, Ci and Cdl are constant due to a fixed semiconductor materials and PBS solution. Therefore, the decrease of hole carrier density (ΔQi) could be transformed by the increase of charge density at solid-liquid interface based on formula (1).

$$\Delta Qi = \frac{\Delta Qh\ Ci}{Ci + Cdl} \quad (1)$$

Consequently, the charge of SARS-CoV-2 N-protein could be characterized by the decrease in holes carrier density and source-drain current. These results confirmed that $I_{DS(max)}$ in transfer characteristics was fairly dependent on the concentration of N-protein in sensing area, which was beneficial for detecting N-protein by H-diamond SGFET biosensor. Furthermore, this prepared H-diamond biosensor had a wide detection range from 10^{-14} to 10^{-5} g/mL with a low limit of detection 10^{-14} g/mL, which is critical for the trace detection of SARS-CoV-2 N-protein.

4. Conclusions

In this study, H-diamond SGFET was developed to detect SARS-CoV-2 N-protein. The characteristic peaks of N-protein antibody and Pyr-NHS in FT-IR spectrum confirmed the modification of H-diamond, EDS spectrum expressed the increase of N and C element on surface. And SEM images intuitively indicated the uniformly distributed Pyr-NHS and antibody on H-diamond surface. The concentration of SARS-CoV-2 N-protein was determined by the changes of transfer characteristics of prepared H-diamond biosensor. A linear relationship between shifts of $I_{DS(max)}$ and Log_{10}(N-protein) was observed with goodness of fit R^2 = 0.90 and sensitivity of 1.98 μA/Log_{10} [concentration of N-protein] at V_{DS} = −500 mV, V_{GS} = −500 mV. In addition, this biosensor had a wide detection range for SARS-CoV-2 N-protein from 10^{-14} to 10^{-5} g/mL and a low limit of detection 10^{-14} g/mL. Therefore, this H-diamond SGFET biosensor could provide potential application for the trace detection of SARS-CoV-2 N-protein.

CRediT authorship contribution statement

Qianwen Zhang: Conceptualization, Methodology, Writing-original

draft. Minghui Zhang: Methodology, Validation. Yuxiang Du: Review & Editing. Bangqiang Xu: Review & Editing. Genqiang Chen: Investigation. Shi He: Visualization. Dan Zhang: Data curation. Qi Li: Methodology. Hong-Xing Wang: Project administration.

Declaration of competing interest

The authors declare that they have no known competing financial interests or personal relationships that could have appeared to influence the work reported in this paper.

Data availability

No data was used for the research described in the article.

Acknowledgments

This work was supported by the Science and Technology Bureau of Xi'an (Grant No. XA2020-YXYJ-0105), Natural Science Basic Research Program of Shaanxi under Grant 2021JQ-062; National Key Research and Development Program of China (No. 2018YFE0125900), National Natural Science Foundation of China (Nos. 61627812, 61804122 and 62074127), China Postdoctoral Science Foundation (Nos. 2019M660256 and 2020M683485), Natural Science Basic Research Program of Shaanxi Province (No. 2023-JC-QN-0763), and Key R&D Program of Shaanxi Province (No. 2021GY-223).

Appendix A. Supplementary data

Supplementary data to this article can be found online at https://doi.org/10.1016/j.diamond.2023.109775.

References

[1] M. Chand, Investigation of novel SARS-COV-2 variant Variant of Concern 202012 / 01 Detection of an epidemiological cluster associated with a new variant of concern Nomenclature of variants in the UK Current epidemiological findings, Public Health Engl. (2020) 1–11.
[2] R.R. Assay, R. Detection, H. Chung, M. Jian, C. Chang, J. Lin, K. Yeh, C. Chen, S. Hsieh, Emergency SARS-CoV-2 variants of concern, Novel Multiplex 10 (2022) 1–10.
[3] R.K. Kakhki, M.K. Kakhki, A. Neshani, COVID-19 target: a specific target for novel coronavirus detection, Gene Rep. 20 (2020) 19–21, https://doi.org/10.1016/j.genrep.2020.100740.
[4] P.I. Kontou, G.G. Braliou, N.L. Dimou, G. Nikolopoulos, P.G. Bagos, Antibody tests in detecting SARS-CoV-2 infection: a meta-analysis, Diagnostics 10 (2020), https://doi.org/10.3390/diagnostics10050319.
[5] R.T. Cai Linlin, L.I.A.N.G. Jiangpeng, C.H.E.N. Libin, X.I.A.N.G. Bin, Research progress in test technique for severe acute respiratory syndrome coronavirus 2, Guangdong J. Anim. Vet. Sci. (2022), https://doi.org/10.19978/j.cnki.xmsy.2022.02.09.
[6] S. Kang, M. Yang, Z. Hong, L. Zhang, Z. Huang, X. Chen, S. He, Z. Zhou, Z. Zhou, Q. Chen, Y. Yan, C. Zhang, H. Shan, S. Chen, Crystal structure of SARS-CoV-2 nucleocapsid protein RNA binding domain reveals potential unique drug targeting sites, Acta Pharm. Sin. B 10 (2020) 1228–1238, https://doi.org/10.1016/j.apsb.2020.04.009.
[7] X.Y. Che, L.W. Qiu, Y.X. Pan, K. Wen, W. Hao, L.Y. Zhang, Y. Di Wang, Z.Y. Liao, X. Hua, V.C.C. Cheng, K.Y. Yuen, Sensitive and specific monoclonal antibody-based capture enzyme immunoassay for detection of nucleocapsid antigen in sera from patients with severe acute respiratory syndrome, J. Clin. Microbiol. 42 (2004) 2629–2635, https://doi.org/10.1128/JCM.42.6.2629-2635.2004.
[8] S. Chen, D. Lu, M. Zhang, J. Che, Z. Yin, S. Zhang, W. Zhang, X. Bo, Y. Ding, S. Wang, Double-antigen sandwich ELISA for detection of antibodies to SARS-associated coronavirus in human serum, Eur. J. Clin. Microbiol. Infect. Dis. 24 (2005) 549–553, https://doi.org/10.1007/s10096-005-1378-7.
[9] P.R. Hsueh, C.L. Kao, C.N. Lee, L.K. Chen, M.S. Ho, C. Sia, X. De Fang, S. Lynn, T. Y. Chang, S.K. Liu, A.M. Walfield, C.Y. Wang, SARS antibody test for serosurveillance, Emerg. Infect. Dis. 10 (2004) 1558–1562, https://doi.org/10.3201/eid1009.040101.
[10] H. Kang, X. Wang, M. Guo, C. Dai, R. Chen, L. Yang, Y. Wu, T. Ying, Z. Zhu, D. Wei, Y. Liu, D. Wei, Ultrasensitive detection of SARS-CoV-2 antibody by graphene field-effect transistors, Nano Lett. 21 (2021) 7897–7904, https://doi.org/10.1021/acs.nanolett.1c00837.
[11] M. Thanihaichelvan, S.N. Surendran, T. Kumanan, U. Sutharsini, P. Ravirajan, R. Valluvan, T. Tharsika, Selective and electronic detection of COVID-19 (Coronavirus) using carbon nanotube field effect transistor-based biosensor: a proof-of-concept study, Mater. Today Proc. 49 (2021) 2546–2549, https://doi.org/10.1016/j.matpr.2021.05.011.
[12] J. Gao, C. Wang, Y. Chu, Y. Han, Y. Gao, Y. Wang, C. Wang, H. Liu, L. Han, Y. Zhang, Graphene oxide-graphene Van der waals heterostructure transistor biosensor for SARS-CoV-2 protein detection, Talanta 240 (2022) 1–7, https://doi.org/10.1016/j.talanta.2021.123197.
[13] X. Zhang, T. Matsumoto, S. Yamasaki, C.E. Nebel, T. Inokuma, N. Tokuda, Inversion - type p - channel diamond MOSFET issues, J. Mater. Res. 36 (2021) 4688–4702.
[14] N.A. Ahmad, R.A. Rahim, B. Rezek, A. Kromka, N.S. Ismail, S.C.B. Gopinath, T. Izak, V. Prochazka, F.N.M. Faudzi, A.S.Z. Abidin, N.N.M. Maidizn, Nanocrystalline diamond electrolyte-gates in field effect transistor for a prolific aptasensing HIV-1 tat on hydrogen-terminated surface, Int. J. Nanoelectron. Mater. 13 (2020) 295–306.
[15] A.R. Ruslinda, S. Tajima, Y. Ishii, Y. Ishiyama, R. Edgington, H. Kawarada, Aptamer-based biosensor for sensitive PDGF detection using diamond transistor, Biosens. Bioelectron. 26 (2010) 1599–1604, https://doi.org/10.1016/j.bios.2010.08.002.
[16] K.S. Song, G.J. Zhang, Y. Nakamura, K. Furukawa, T. Hiraki, J.H. Yang, T. Funatsu, I. Ohdomari, H. Kawarada, Label-free DNA sensors using ultrasensitive diamond field-effect transistors in solution, Phys. Rev. E - Stat. Nonlinear Soft Matter Phys. 74 (2006) 1–7, https://doi.org/10.1103/PhysRevE.74.041919.
[17] W. Yang, K.R. Ratinac, S.R. Ringer, P. Thordarson, J.J. Gooding, F. Braet, Carbon nanomaterials in biosensors: should you use nanotubes or graphene, Angew. Chem. Int. Ed. 49 (2010) 2114–2138, https://doi.org/10.1002/anie.200903463.
[18] W. Wang, C. Hu, F.N. Li, S.Y. Li, Z.C. Liu, F. Wang, J. Fu, H.X. Wang, Reprint of «palladium ohmic contact on hydrogen-terminated single crystal diamond film», Diam. Relat. Mater. 63 (2016) 175–179, https://doi.org/10.1016/j.diamond.2016.01.019.
[19] C.Y. Panicker, H.T. Varghese, A. John, D. Philip, K. Istvan, G. Keresztury, FT-IR, FT-Raman and FT-SERS spectra of 4-aminosalicylic acid sodium salt dihydrate, Spectrochim. Acta - Part A Mol. Biomol. Spectrosc. 58 (2002) 281–287, https://doi.org/10.1016/S1386-1425(01)00541-8.
[20] C. Zhai, W. Li, L. Ma, L. Wu, Y. Wu, Structural and orientational studies of chiral N-[4(1-pyrene)butyroyl]-phenylalanine in cast film, Spectrochim. Acta - part a MolBiomol. Spectrosc. 61 (2005) 2713–2719, https://doi.org/10.1016/j.saa.2004.10.029.
[21] A. Adochitei, G. Drochioiu, Rapid characterization of peptide secondary structure by FT-IR spectroscopy, Rev. Roum. Chim. 56 (2011) 783–791.
[22] A. Schwaighofer, M. Montemurro, S. Freitag, C. Kristament, M.J. Culzoni, B. Lendl, Beyond Fourier transform infrared spectroscopy: external cavity quantum cascade laser-based mid-infrared transmission spectroscopy of proteins in the amide I and amide II region, Anal. Chem. 90 (2018) 7072–7079, https://doi.org/10.1021/acs.analchem.8b01632.
[23] W. Wang, Protein aggregation and its inhibition in biopharmaceutics, Int. J. Pharm. 289 (2005) 1–30, https://doi.org/10.1016/j.ijpharm.2004.11.014.
[24] B. Rezek, C.E. Nebel, Electronic properties of plasma hydrogenated diamond surfaces: a microscopic study, Diam. Relat. Mater. 15 (2006) 1374–1377, https://doi.org/10.1016/j.diamond.2005.10.002.
[25] K. Xing, P. Aukarasereenont, S. Rubanov, A. Zavabeti, D.L. Creedon, W. Li, B. C. Johnson, C.I. Pakes, J.C. McCallum, T. Daeneke, D.C. Qi, Hydrogen-terminated diamond MOSFETs using ultrathin glassy Ga2O3Dielectric formed by low-temperature liquid metal printing method, ACS Appl. Electron. Mater. (2022), https://doi.org/10.1021/acsaelm.2c00093.
[26] Y.F. Wang, W. Wang, H.N. Abbasi, X. Chang, X. Zhang, T. Zhu, Z. Liu, W. Song, G. Chen, H.X. Wang, LiF/AlO as dielectrics for MOSFET on single crystal hydrogen-terminated diamond, IEEE Electron Device Lett. 41 (2020) 808–811, https://doi.org/10.1109/LED.2020.2990118.
[27] Y.J. Xu Benjin, Du. Fan Lei, Xuan Yan Miao, Li Jing, Li Zhuoxi, Wu. Chen Xiaocong, Men Jie Huiwen, Liu Ling, Yang Yanan, Tang Wenting, Yu. Kou Yanqi, Junxiao Xu Benjin, Du. Fan Lei, Xuan Yan Miao, Li Jing, Li Zhuoxi, Chen Xiaocong, Wu Huiwen, Men Jie, Liu Ling, Bioinformatic analysis and prokaryotic expression of the structure and function of COVID-19 nucleocapsid protein, Chin. J. Immunol. 37 (2021) 1–25.
[28] S.W. Lee, S. Kim, J. Malm, O.C. Jeong, H. Lilja, T. Laurell, Improved porous silicon microarray based prostate specific antigen immunoassay by optimized surface density of the capture antibody, Anal. Chim. Acta 796 (2013) 108–114, https://doi.org/10.1016/j.aca.2013.06.041.
[29] J.W. Chung, J.M. Park, R. Bernhardt, J.C. Pyun, Immunosensor with a controlled orientation of antibodies by using NeutrAvidin-protein A complex at immunoaffinity layer, J. Biotechnol. 126 (2006) 325–333, https://doi.org/10.1016/j.jbiotec.2006.05.010.
[30] F. Maier, M. Riedel, B. Mantel, J. Ristein, L. Ley, Origin of surface conductivity in diamond, Phys. Rev. Lett. 85 (2000) 3472–3475, https://doi.org/10.1103/PhysRevLett.85.3472.